Source attribution of near-surface ozone trends in the United States during 1995–2019

Pengwei Li[1], Yang Yang[1*], Hailong Wang[2], Su Li[1], Ke Li[1], Pinya Wang[1], Baojie Li[1], Hong Liao[1]

[1]Jiangsu Key Laboratory of Atmospheric Environment Monitoring and Pollution Control, Jiangsu Collaborative Innovation Center of Atmospheric Environment and Equipment Technology, School of Environmental Science and Engineering, Nanjing University of Information Science and Technology, Nanjing, Jiangsu, China

[2]Atmospheric Sciences and Global Change Division, Pacific Northwest National Laboratory, Richland, Washington, USA

*Correspondence to yang.yang@nuist.edu.cn

Abstract

Emissions of ozone (O_3) precursors in the United States have decreased in recent decades, and near-surface O_3 concentrations showed a significant decrease in summer but an increase in winter. In this study, an O_3 source tagging technique is utilized in a chemistry-climate model to investigate the source contributions to O_3 mixing ratios in the U.S. from various emitting sectors and regions of nitrogen oxides (NO_x) and reactive carbon species during 1995–2019. We show that domestic emission reductions from energy and surface transportation are primarily responsible for the decrease in summertime O_3 during 1995–2019. However, in winter, the emission control also weakens the NO_x titration process, resulting in considerable increases in O_3 levels from natural sources. Additionally, increases in aviation and shipping emissions and transpacific transport of O_3 from Asia largely contribute to the winter O_3 increase. We also found that changes in large-scale circulation favoring O_3 transport from upper atmosphere and foreign transport from Asia also explain 15% of the increase in the U.S. near-surface O_3 levels in winter.

1. Introduction

Ozone (O_3) near the surface has a significant impact on air quality and public health (Haagen-Smit, 1952; Fleming et al., 2018). Since the increase in anthropogenic emissions of O_3 precursors from preindustrial times, O_3 has now become the third most important anthropogenic greenhouse gas in the troposphere (Myhre et al., 2013). Major sources of O_3 in the troposphere include the transport from the stratosphere and formation through photochemical reactions within the troposphere involving two chemically distinct groups of precursors: nitrogen oxides (NO_x) and reactive carbon species, including carbon monoxide (CO), methane (CH_4), and non-methane volatile organic compounds (NMVOCs) (Atkinson, 2000). O_3 precursors come from a variety of sectors, and its relatively long lifetime of about 22 days (Stevenson et al. 2006) favors the long-range transport of O_3. Due to the nonlinearity of the O_3 production and its associated dependence on precursor emissions (Seinfeld and Pandis, 2006), attributing O_3 pollution to its sources is complicated.

Since the 1980s, O_3 precursor emissions have significantly reduced in the United States (Duncan et al., 2016; Xing et al., 2013; Zhang et al., 2016; Zhang et al., 2021). However, due to the nonlinear production chemistry of O_3, complex seasonal meteorological influence, and long-range transport from foreign source regions, domestic emissions reductions do not imply a decrease in seasonal and annual O_3 concentrations. According to remote surface measurements (Cooper et al., 2020) and aircraft observations (Gaudel et al., 2020), the Sixth Assessment Report of the Intergovernmental Panel on Climate Change (Szopa et al., 2021) showed a decreasing trend in annual mean O_3 concentrations in the western U.S. but an increasing trend in the eastern U.S. since the mid-1990s. On the seasonal timescale, surface observations and modeling results showed that O_3 concentrations over the U.S. had decreased

in summer due to the reductions in domestic anthropogenic emissions and increased in winter related to the weakened NO_x titration since the late 1980s (Cooper et al., 2012; Lin et al., 2017). It also shows that the increased background O_3, especially due to an increased transport from Asia, can partly offset the benefit of domestic emissions control over the western U.S. in summer.

Source apportionment is a useful method for quantifying contributions to air pollutants from specific source regions and/or sectors, which is beneficial to emission control strategies (Yang et al., 2018). One method of obtaining an O_3 source-receptor relationship is to zero out or perturb emissions from a given source region or sector in sensitivity simulations along with a baseline simulation, which gives information about the response of O_3 to changes in precursor emissions (e.g., Fiore et al., 2009; Hoor et al., 2009). However, emission perturbation method requires many additional model simulations when being used to estimate the impacts of changes in multiple sources (Koo et al., 2009; Wang et al., 2014). The perturbation method may invalidate the assumption of a linear relationship between the magnitude of the emission perturbation and the magnitude of the O_3 change considering the nonlinearity in O_3 chemistry, especially if large perturbations (e.g. zeroing out regional or sector-wide emissions) are used. The tagging approach produces information about the contribution of precursor emissions to the total amount of O_3 (Butler et al., 2020). The perturbation and tagging methods are two different methods answering different scientific questions, with the first for the impacts and the last for the contributions (Grewe et al. 2010, Emmons et al. 2012, Clappier et al. 2017 and Thunis et al., 2019). Both of these two methods can be used for specific purpose to provide a comprehensive understanding of source-receptor relationships between precursor emissions and O_3 concentrations.

The source tagging method has been widely adopted in regional air quality

models to examine the O_3 attribution in the U.S., China, and/or Europe (Gao et al., 2016; Collet et al., 2018; Lupaşcu and Butler, 2019). In some regional models, O_3 apportionment is based on the ratio of chemical indicators to determine the regime of O_3 generation (e.g., VOC-limited or NO_x-limited regimes) and then attribute the generation of O_3 to the tag carried by a certain precursor (VOCs or NO_x), which however cannot simultaneously attribute O_3 production to NO_x and VOCs, respectively (Dunker et al., 2002; Kwok et al., 2015), while some models do not use the chemical indicators (Lupaşcu and Butler, 2019; Mertens et al., 2020). In addition, due to the limitation in domain size of regional air quality models, they are difficult to account for contributions of intercontinental transport from several sources outside the model domain. Recently, O_3 tagging techniques have been implemented in the global models (e.g., Sudo and Akimoto, et al., 2007; Zhang et al., 2008; Emmons et al., 2012; Grewe et al. 2017; Butler et al., 2018; Han et al., 2018; Bates and Jacob, 2020). However, in many global models, O_3 is tagged by the production regions rather than the precursor emission regions, so that O_3 can only be attributed to the area where O_3 is generated, rather than the source of precursor emissions.

Here, based on a state-of-the-art tagging system implementation in a global chemistry–climate model, the trends of near-surface O_3 mixing ratios in the U.S. during 1995–2019 and the source attributions of the O_3 variations to various emission sectors and regions of NO_x and reactive carbon species are investigated in this study. Mechanisms of explaining the O_3 trends that involve changes in anthropogenic emissions and large-scale circulations are also explored.

2. Methods

2.1 Model Description

Tropospheric O_3 mixing ratios are simulated using the Community Atmosphere Model version 4 with Chemistry (CAM4-chem) (Lamarque et al.,

2012; Tilmes et al., 2015), which is the atmospheric chemistry component of the Community Earth System Model (CESM), at a horizontal resolution of 1.9° latitude by 2.5° longitude with 26 vertical levels extending to 40 km above the surface. The height of bottom layer is about 120 m and there are about 4 layers under 2 km. The model configuration uses a comprehensive tropospheric chemistry mechanism based on the Model for Ozone and Related chemical Tracers version 4 (MOZART-4) (Emmons et al., 2010, 2012). Model configurations simulate wet deposition of gas species using the Neu and Prather (2011) scheme. Dry deposition is represented following the resistance approach originally described in Wesely (1989). Stratosphere-troposphere exchange of O_3 is treated by setting O_3 to stratospheric values as their climatological means over 1996–2005 at the tropopause (Lamarque et al., 2012), which is affected by atmospheric circulation and experiences the same loss rates as O_3 in the troposphere (Tilmes et al., 2016). Sea surface temperatures and sea ice concentrations in our simulations are prescribed at present-day climatological conditions. The zonal and meridional wind fields are nudged towards the MERRA-2 (Modern Era Retrospective-Analysis for Research and Applications Version 2) reanalysis (Gelaro et al., 2017) at a 6-hourly relaxation timescale in this study to better constrain large-scale circulations by observations. The CAM4-chem performance in simulating tropospheric O_3 and precursors has been fully evaluated in Tilmes et al. (2015).

2.2 Ozone Source Tagging Technique

The novel O_3 source tagging technique implemented in the model was developed by Butler et al. (2018), which can provide a separate source apportionment of tropospheric O_3 to the two distinct groups of precursor emissions, i.e., NO_x and reactive carbon (CO, CH_4 and NMVOCs). The portion of tropospheric O_3 that is attributable to the stratosphere-troposphere exchange can also be quantified using this unique tagging technique. The source

attribution of O_3 requires two separate model runs with the tagging applied to NO_x and reactive carbon species, respectively. Details of the O_3 tagging technique are described in Butler et al. (2018).

In this study, near-surface O_3 is attributed to emission sectors and regions. Emissions from individual sectors, including agriculture (AGR), energy (ENE), industry (IND), residential, commercial and other (RCO), surface transportation (TRA), waste management (WST), international shipping (SHP) and biomass burning (BMB) emissions, as well as chemical production in the stratosphere (STR) and extra chemical production (XTR, a small amount of O_3 produced due to the self-reaction of OH radicals and the reactions of HO_2 with certain organic peroxy radicals) are tagged for both NO_x and reactive carbon species. Aircraft (AIR), soil (SOIL) and lightning (LGT) sources are separately tagged for NO_x emissions, while solvents (SLV) and biogenic (BIO) sources are separately tagged for NMVOCs emissions.

For the regional source attribution, we separately tag anthropogenic sources from Africa (AFR), Central America (CAM), Europe (EUR), Middle East (MDE), North America (NAM), East Asia (EAS), South Asia (SAS), Southeast Asia (SEA) and rest of the world (ROW) (see Fig. 1 for the region map) and natural sources (BMB, SOIL, LGT, BIO, STR and XTR). Additional tags for methane (CH_4) and carbon monoxide (CO) are applied in both of the reactive carbon tagging simulations that are used to attribute O_3 to emission sectors and regions. We do not tag CH_4 by individual sources and the contributions of CH_4 from various sources are lumped in this study. It is because CH_4 has a relative long lifetime in the troposphere and it is well mixed in the troposphere due to its exceptionally low reactivity, which can contribute to O_3 formation at any location in the troposphere where photochemical conditions are favorable (Fiore et al., 2008). CO also has a longer lifetime and lower reactivity than most NMVOCs. The lumped CO is tagged in the simulations for emission sectors, but not

specifically tagged in the simulations for emission regions due to the computational limit.

2.3 Emissions and Observation

The global anthropogenic emissions, including NO_x, CO, NMVOCs, SO_2, and NH_3, over 1990–2019 are from the Community Emissions Data System (CEDS) version 20210205 (Hoesly et al., 2018) (See Table S1 and Figs. S1–S3). Biomass burning emissions are obtained from the CMIP6 (Coupled Model Intercomparison Project Phase 6) over 1990–2014 (van Marle et al., 2017) and the emissions for the following five years (2015–2019) are interpolated from the SSP2-4.5 forcing scenario (O'Neill et al., 2016). NO_x emitted from soils and biogenic NMVOCs from vegetation are prescribed as in Tilmes et al. (2015) and are kept at the present-day (2000) climatological levels during simulations. Lightning emissions of NO_x are estimated online using the parameterization based on simulated cloud top heights from Price et al. (1997), which is scaled to provide a global annual emission of 3–5 Tg N yr^{-1} (Lamarque et. al., 2012). CH_4 is fixed at a global average level of 1760 parts per billion (ppb, volume ratio in this study) during simulations.

Many studies have reported that the previous CEDS version 20160726 (hereafter $CEDS_{2016}$) has large biases in the regional emission estimates (e.g., Cheng et al., 2021; Fan et al., 2018). In this study, the CEDS version 20210205 is used (hereafter $CEDS_{2021}$), which builds on the extension of the CEDS system described in McDuffie et al. (2020) and extends the anthropogenic emissions to year 2019. It updates country-level emission inventories for North America, Europe and China and has considered the significant emission reductions in China since the clean air actions in recent years. The global total NO_x emission from $CEDS_{2021}$ is lower than that of $CEDS_{2016}$ after 2006 and it shows a fast decline since then. In 2014, the global total anthropogenic emission of NO_x in $CEDS_{2021}$ is about 10% lower than the $CEDS_{2016}$ estimate.

This difference is mainly reflected in the NO_x emissions in China and India. $CEDS_{2021}$ has a lower estimate of the global NMVOCs emission than $CEDS_{2016}$ by more than 10% during the recent decades, attributed to lower emissions from Africa, Central and South America, the Middle East and India. The using of the $CEDS_{2021}$ emission inventory in this study could reduce the contributions of NO_x emissions from East Asia and South Asia to the U.S. O_3 mixing ratios and trends, as compared to $CEDS_{2016}$. However, recent study reported a difference in aviation emission distribution of NO_x between CMIP5 and CMIP6 related to an error in data pre-processing in CEDS, leading to a northward shift of O_3 burden in CMIP6 (Thor et al., 2023). Therefore, the contribution of the aircraft emissions of NO_x to the O_3 mixing ratios could be overestimated at high latitude regions.

Surface O_3 measurements in the U.S. are obtained from the U.S. Environmental Protection Agency (EPA). Linear trends of surface O_3 are calculated separately for boreal summer (June-July-August, JJA) and winter (December-January-February, DJF). Seasonal mean for any site that has less than 50% data availability in any month of a season is discarded following Lin et al. (2017). O_3 trends is calculated only when the seasonal data availability is greater than 85% during the analyzed period (more than 22 years). Trends in this study are calculated based on the linear least-squares regressions and the statistical significance is identified through the F test with the 95% confidence level.

2.4 Experimental Design

In this study, four groups of experiments are conducted, each group includes both NO_x tagging simulation and reactive carbon tagging simulation. Two BASE experiment groups include simulations with emission sectors and regions, respectively, tagged for the two chemical distinct precursors. The BASE experiments are performed with time-varying anthropogenic emissions

and winds nudged to MERRA-2 reanalysis. The other two groups of sensitivity experiments (MET) are the same as BASE experiments, except that the anthropogenic emissions are held at year 2019 level during simulations. All experiments are performed over 1990–2019, with the first 5 years treated as model spin-up and the last 25 years used for analysis. The BASE experiments are analyzed to quantify the source attributions of O_3 in the U.S., unless stated otherwise. We note that although the wind fields are nudged at a 6-hourly relaxation timescale, the atmospheric dynamics could also be slightly different between simulations, leading to the slight changes in the contributions from the same tags between simulations.

2.5 Model Evaluation

Figure 2 compares the simulated near-surface O_3 mixing ratios with those from observations in 1995 and 2019, respectively. In general, the model overestimates O_3 mixing ratios in the U.S. in both summer and winter by 10–40%. It can capture the seasonal pattern of O_3 that high mixing ratios in summer and low mixing ratios in winter. The spatial distributions can also be roughly captured by the model, with statistically significant correlation coefficients between simulations and observations in the range of 0.21–0.45. From 1995 to 2019, the O_3 mixing ratios in the U.S. decreased in summer and increased in winter presented in observations. The model can produce the sign of the changes, but has large biases in magnitudes, which will be discussed in the following section.

3 Results

3.1 Ground-level ozone trends in the U.S.

Emissions of O_3 precursors have substantially reduced since 1995 in both the western U.S. (WUS, 100–125°W, 30–45°N) and eastern U.S. (EUS, 70–100°W, 30–45°N), primarily owning to the reductions in anthropogenic

emissions (Figs. S1–S3). However, the simulated annual near-surface O_3 mixing ratios present opposite trends between WUS and EUS, with increases in EUS but weak decreases in WUS, which also exist in observations (Fig. 3a).

The simulated contrasting trends in annual mean O_3 mixing ratios between the WUS and EUS are dominated by the strong decreases in O_3 mixing ratios in summer across the U.S. (Fig. 3b) and increased O_3 levels in winter over the central-eastern U.S. during 1995–2019 (Fig. 3c). The opposite trends between summer and winter have also been noted in many previous studies (e.g., Copper et al., 2012; Lin et al., 2017, Jaffe et al., 2018). The model reproduces the observed O_3 trend over EUS in summer and roughly captures the O_3 trend over WUS in winter (Table 1). The decreasing trend over WUS in summer and increasing trend over EUS in winter, however, are largely overestimated in the model, partly attributed to the coarse model resolution. The model also tends to overestimate the weakening of NO_x titration in winter, leading to the biases. For spring and autumn, they are the transition between summer and winter, having the similar spatial pattern of O_3 trends as annual average, and will not be concerned in this study.

3.2 Source attribution of ozone trends to emission sectors

During 1995–2019, summer and winter NO_x emissions from energy and surface transport sectors have significantly decreased in both WUS and EUS, followed by industry and residential sectors, while those from aircraft have increased slightly (Fig. 4). Emissions of NMVOCs from surface transportation, solvents, industry, residential and waste sectors have decreased across the U.S., while those from energy and agriculture have increased. CO emissions have also significantly decreased over this time period.

The time series of the source sector contributions to O_3 mixing ratios from NO_x and reactive carbon emissions are shown in Fig. 5 and the O_3 trends in the U.S. attributed to different emission source sectors are shown in Fig. 6. In

summer, the O_3 attributed to NO_x emissions from energy and surface transportation decreased at the rate of 2.0±0.2 and 1.6±0.2 ppb/decade in WUS and 3.2±0.2 and 1.7±0.2 ppb/decade in EUS, respectively (Figs. 6a and 6c). On the contrary, the O_3 contributed by aircraft NO_x emissions increased by 0.4 ± 0.0 ppb/decade in both WUS and EUS. Along with the reductions in anthropogenic emissions, natural emissions are becoming increasingly important as sources for O_3 formation near the surface. Although NO_x emissions from soil are held at the present-day climatological levels, they account for 0.7±0.1 and 1.7±0.1 ppb/decade increase in WUS and EUS, respectively, during 1995–2019, related to the changing O_3 production efficiency under the more NO_x-sensitive condition. Note that, during 1995–2019, the molar ratio (mol N /mol C) of emitted NO_x to NMVOCs reduced from 0.11 to 0.07 in WUS and from 0.14 to 0.07 in EUS, confirming the enhanced NO_x-sensitive condition during the analyzed time period. In recent decades, global emissions from international shipping have increased rapidly (Eyring et al., 2005; Müller-Casseres et al., 2021), but have declined near the coast of the United States. Due to a strong chemical sink associated with photolysis of O_3 with subsequent production of hydroxyl radical (OH) from water vapor in summer (Johnson et al., 1999), the effect of increased international shipping emissions over the remote ocean regions on the continental U.S. was blunted. But the increase in shipping emissions inland tends to increase O_3 mixing ratios in eastern U.S. (Fig. S4).

In summer, biogenic sources dominate the emissions of NMVOCs in the U.S. (Fig. S3). As the O_3 decreases, mainly due to the reductions in domestic NO_x emissions, the contributions from biogenic emissions of NMVOCs have a decreasing trend in the U.S. during 1995–2019 (Figs. 6b and 6d), even though biogenic emissions were fixed during simulations. This also applies to CH_4, of which the mixing ratio was kept constant. This does not actually mean that CH_4

317 and biogenic NMVOCs themselves contributed to the overall O_3 trend through
318 changing the precursor levels since they were kept constant during simulations;
319 rather, mainly due to the reductions in NO_x emissions, O_3 production efficiency
320 by reactive carbon species decreases, leading to decreasing trends of O_3
321 contribution by CH_4 and biogenic NMVOCs. In conjunction with NO_x emission
322 reductions, decreases in NMVOCs emissions from surface transportation and
323 industry sectors contribute negative O_3 trends of –0.3±0.0 and –0.1±0.0
324 ppb/decade, respectively, in both WUS and EUS in summer (Figs 6b and 6d),
325 which are offset by the increases in NMVOCs emissions from energy and
326 agriculture sectors. Although the O_3 production efficiency of CO is relatively low,
327 the contributions of CO to O_3 mixing ratios largely decreased with trends of –
328 0.6±0.1 and –0.5±0.1 ppb/decade in WUS and EUS, respectively, due to the
329 massive reduction in anthropogenic emissions of CO (Fig. S1).
330 In winter, through the weakened NO_x titration process (Gao et al., 2013;
331 Simon et al., 2015), the NO_x emission control causes an increase in O_3 levels
332 during 1995–2019, especially the contribution from surface transportation
333 (0.4±0.0 ppb/decade in WUS and 0.8±0.1 ppb/decade in EUS) (Figs. 6e and
334 6g). Although aircraft NO_x emissions slightly increased, O_3 attributed to aircraft
335 NO_x emissions shows positive trends as large as 0.4±0.0 and 0.6±0.0
336 ppb/decade in WUS and EUS, respectively. It is because aircraft emissions are
337 injected directly into the upper troposphere and lower stratosphere in a low
338 ambient NO_x condition and have a much higher O_3 enhancement efficiency
339 than surface emissions (Hodnebrog et al., 2011). It can be confirmed that the
340 NO_x from aircraft contributes to the increase in O_3 mixing ratios at 250 hPa in
341 high latitude regions of the Northern Hemisphere during 1995–2019 (Fig. S5).
342 The decrease in near-shore shipping emissions weakened the NO_x titration,
343 together with the weakened O_3 chemical sink from water vapor in winter,
344 leading to large increasing trends of O_3 by 0.8±0.1 and 1.0±0.1 ppb/decade,

respectively, in the WUS and EUS during 1995–2019. Although most natural emissions do not change during the simulations, the net O_3 chemical production is more sensitive to NO_x under the emission control condition, resulting in the increasing O_3 trends contributed by the soil and lightning NO_x emissions. Due to the weakened NO_x titration in winter, the contribution of stratospheric intrusion increases at a rate of 0.6±0.1 and 1.0±0.1 ppb/decade over WUS and EUS, respectively, when stratospheric contribution to the near-surface O_3 is relatively high (Butler et al., 2018). Along with the weakened NO_x titration, contributions from reactive carbon emissions to the near-surface O_3 in the U.S. also increase for most species and sectors (Figs. 6f and 6h).

3.3 Source attribution of ozone trends to emission regions

Time series of the source region contributions to near-surface O_3 mixing ratios are shown in Fig. 7 and the O_3 trends in the U.S. attributed to different emission source regions are presented in Fig. 8. In summer, domestic anthropogenic NO_x emissions (excluding those from soil) within North America account for 49% of the near-surface O_3 mixing ratio averaged over the U.S. (WUS+EUS) in 1995–2019. The domestic emission reduction is the dominant factor causing the decline in surface O_3 mixing ratios, with contributions of –4.4±0.2 and –5.7±0.3 ppb/decade to the trends over WUS and EUS, respectively, during 1995–2019 (Figs. 8a and 8c). Reductions in the NMVOCs emissions from North American anthropogenic sources also decrease O_3 mixing ratios (Figs. 8b and 8d), accompanying with the domestic NO_x emission control. The increase in NO_x emissions from Asia contributes 0.7±0.1 ppb/decade to the total O_3 increasing trend in WUS, partly offsetting the negative impact of domestic emission reductions, but has a weak impact in EUS, which is consistent with previous studies (Lin et al., 2017).

In winter, domestic anthropogenic NO_x emissions only account for 19% of the surface O_3 mixing ratio in the U.S. over 1995–2019, while NO_x sources from

lightning, rest of the world (mainly from the international shipping), and Asia contribute 17%, 14%, and 11%, respectively. O_3 from stratospheric intrusion contributes 21% of the near-surface O_3 in the U.S. in winter. During 1995–2019, the significant increase in wintertime surface O_3 mixing ratios are not directly linked to the reductions in domestic anthropogenic emissions (Figs. 8e and 8g). However, the domestic emission control weakens the NO_x titration, resulting in considerable increases in O_3 originating from the natural sources, including O_3 from stratospheric intrusion, lightning and soil emissions. The natural sources combined contribute to positive O_3 trends of 1.2±0.2 and 2.4±0.3 ppb/decade in WUS and EUS, respectively. If the O_3 increase is attributed to NMVOCs emissions, the combined natural source contribution is even larger (1.4±0.2 in WUS and 2.5±0.2 ppb/decade in EUS) (Figs. 8f and 8h). O_3 produced by CH_4 increases at rates of 1.3±0.1 and 2.1±0.1 ppb/decade in WUS and EUS, respectively, due to the weakened NO_x titration. Increases in aviation and shipping emissions together explain the 1.2±0.1 and 1.5±0.1 ppb/decade of O_3 trends in WUS and EUS, respectively (Figs. 6e and 6g). Long-range transport of O_3 produced from Asian NO_x emissions enhances the wintertime O_3 increasing trends by 0.9±0.1 and 1.2±0.1 ppb/decade in WUS and EUS, respectively, which are equally contributed by sources from East Asia, South Asia, and Southeast Asia (Figs. 8e and 8g).

3.4. Impact of variations in large-scale circulations on ozone trends

Many studies have reported that O_3 spatial distribution is strongly modulated by changes in large-scale circulations (e.g., Shen and Mickley, 2017; Yang et al., 2014, 2022). Based on our MET experiments with anthropogenic emissions kept unchanged, the changes in large-scale circulations show a weak influence on the U.S. O_3 trends in summer (Fig. 9a) but cause a significant O_3 rise in the central U.S. in winter (Fig. 9b). Averaged over the U.S., the near-surface O_3 mixing ratio in winter increases at the rate of 0.7±0.3 ppb/decade

during 1995–2019 in MET experiments. It suggests that the variation in large-scale circulations is responsible for 15% of the increasing trend in wintertime O_3 mixing ratio by 4.7±0.3 ppb/decade in the U.S. during 1995–2019 simulated in BASE experiment.

The changes in atmospheric circulation pattern support the above finding. Compared to 1995–1999, anomalous northerly winds locate over high latitudes of North America in 2015–2019 (Fig. 9c), strengthening the prevailing northerly winds in winter. In addition, an anomalous subsidence occurs over the central U.S. in 2015–2019, compared to 1995–1999 (Fig. 9d). The anomalous subsidence transport O_3 from high altitudes and even stratosphere to the surface and the strengthened winds transport O_3 from remote regions (e.g., O_3 produced by Asian NO_x emission) to the central U.S., both contributing to 0.2±0.1 ppb/decade of the O_3 increase over the U.S. (Fig. 10). The finding is consistent with Lin et al. (2015) that variations in the circulation facilitate O_3 transport from upper altitudes to the surface, as well as foreign contributions from Asia. The anomalous atmospheric circulation is likely linked to the location of the midlatitude jet stream, which is influenced by ENSO cycle.

4. Conclusions and discussions

Using a global chemistry–climate model equipped with an O_3 source tagging technique, we examine the long-term trends and source apportionment of O_3 in the continental U.S. over 1995–2019 to various emission source sectors and regions in this study. This model can capture the O_3 decreasing trend over the EUS in summer and increasing trend over the WUS in winter during this time period, but largely overestimates the decreasing trend over WUS in summer and increasing trend over EUS in winter.

In summer, our simulation results show that the decline in surface O_3 is dominated by the rapid reductions in NO_x emissions from energy and surface

transportation sectors, contributing to O_3 decreases at a rate of –2.0 and –1.6 ppb/decade in WUS and –3.2 and –1.7 ppb/decade in EUS, respectively. As the anthropogenic NO_x decreases, the more NO_x-sensitive condition leads to a positive O_3 trend of 0.7 and 1.7 ppb/decade in WUS and EUS, respectively, contributed by the NO_x emissions from soil. Due to the reductions in NO_x emissions, the O_3 production efficiency by reactive carbon species also decreased, leading to the decreasing contributions to O_3 from reactive carbon species in summer during 1995–2019. Even though biogenic NMVOCs emissions and CH_4 mixing ratio were fixed during simulations, their contributions also decreased related to the weakened O_3 production efficiency by these precursors. Source region tagging suggests that the domestic emission reductions are primarily responsible for the decreasing trend in summertime near-surface O_3 mixing ratios in the U.S. during 1995–2019.

The mechanisms of wintertime O_3 increases over the U.S. are more complicated. First, the domestic emission control weakens the NO_x titration, resulting in considerable increases in O_3 originating from natural sources, including O_3 from stratospheric intrusion, lightning, soil and biogenic emissions. The natural sources combined contribute a positive O_3 trend of more than 1 and 2 ppb/decade in WUS and EUS, respectively. Second, increases in aviation and shipping emissions together explain the 1.2 and 1.5 ppb/decade of O_3 trends in WUS and EUS, respectively. Third, long-range transport of O_3 produced from Asian NO_x emissions enhances the wintertime O_3 increasing trends by 0.9 and 1.2 ppb/decade in WUS and EUS, respectively. Fourth, the variation of horizontal and vertical transport O_3 associated with the changes in large-scale circulation contributes to the near-surface O_3 increases over the U.S. by 15% in winter during 1995–2019.

Compared to observations, the decreasing trend of O_3 mixing ratios over WUS in summer and increasing trend over EUS in winter are overestimated in

457 the CAM4-chem model. Because most O_3 monitors are located in urban areas
458 and these areas generate strong O_3 during the day and have strong oxidation
459 titration at night, the daily and grid averaged O_3 mixing ratios output by the
460 model could be inconsistent with the urban observations. The overestimate of
461 O_3 trend in the EUS might be related to a potential biased model representation
462 of vertical mixing in winter. Large uncertainties existing in the emissions also
463 result in the biases in the O_3 simulation. Lin et al. (2017) found that the
464 contribution from increasing Asian emissions offset that from the U.S. emission
465 reductions, resulting in a weak O_3 trend in WUS. In this study, the Asian NO_x
466 emissions only contribute to 0.6 ppb/decade of the total positive trend in WUS
467 in summer, much lower than the 3.7 ppb/decade decrease attributable to the
468 domestic emission reductions, suggesting that the Asian contribution to the O_3
469 trends in WUS is possibly underestimated in this study. We also found that the
470 model did not capture the significant increase in summertime O_3 levels in China
471 in recent years, which could explain the low contribution from Asian sources.
472 Additionally, international shipping can have a disproportionately high influence
473 on tropospheric O_3 due to the dispersed nature of NO_x emissions (Butler et al.,
474 2020; Kasibhatla et al., 2000; von Glasow et al., 2003), together with the
475 weakened NO_x titration, resulting in the overestimation of O_3 trends. The fixed
476 CH_4 mixing ratio during simulations also biased the modeled O_3 trends, which
477 deserves further investigation with the varying CH_4 levels in future studies. The
478 coarse model resolution also contributed to the biases. The overestimate of O_3
479 trend over EUS in winter, likely related to the bias in NO_x titration, implies the
480 overestimate of source contributions to the trends in magnitude.

481 Compared with Butler et al. (2018), the simulation in this study shares
482 similar source sector contributions to the zonal average of O_3 mixing ratios at
483 the surface and 400 hPa in 2010 (Figs. S7 and S8 in this study and Figs. 5 and
484 6 in Butler et al. (2018)). The contributions from the stratosphere and lightning

485 NO_x are relatively higher in this study than Butler et al. (2018). This may be
486 related to the different anthropogenic emission inventories used, causing
487 different O_3 production/loss efficiencies by natural precursors. When comparing
488 the contributions from different source regions to surface O_3 mixing ratios in
489 North America, NO_x emissions from East Asia, South Asia, North America, and
490 Europe contributed 2.2, 1.1, 8.3, and 0.7 ppb of the surface O_3 in North America,
491 respectively (Fig. S9) in this study, which are also similar to those from Fig. 4 in
492 Butler et al. (2020). Both studies show the contributions of anthropogenic
493 NMVOCs to surface O_3 mixing ratios in North America are less than 10 ppb.
494
495

Author contributions. YY designed the research; PL and SL performed simulations; PL analyzed the data. All authors including HW, KL, PW, BL, and HL discussed the results and wrote the paper.

Code and data availability. The CESM is maintained by NCAR and is provided freely to the community. The ozone tagging code has been described by Butler et al. (2018). The MERRA-2 reanalysis data are from NASA GESDISC data (https://goldsmr5.gesdisc.eosdis.nasa.gov/data/MERRA2/M2I6NVANA.5.12.4/, last access: 1 August 2022). The surface O_3 measurements in U.S. are obtained from the U.S. Environmental Protection Agency (https://aqs.epa.gov/aqsweb/airdata/download_files.html#Daily, last access: 1 August 2022). The modeling results are made available at https://doi.org/10.5281/zenodo.6891316 (last access: 1 August 2022).

Acknowledgments

HW acknowledges the support by the U.S. Department of Energy (DOE), Office of Science, Office of Biological and Environmental Research (BER), as part of the Earth and Environmental System Modeling program. The Pacific Northwest National Laboratory (PNNL) is operated for DOE by the Battelle Memorial Institute under contract DE-AC05-76RLO1830.

Financial support. This study was supported by the National Key Research and Development Program of China (grant 2020YFA0607803), Jiangsu Science Fund for Distinguished Young Scholars (grant BK20211541) and the Jiangsu Science Fund for Carbon Neutrality (grant BK20220031).

Competing interests. The authors declare that they have no conflict of interest.

References

Atkinson, R.: Atmospheric chemistry of VOCs and NO_x, Atmos. Environ., 34, 2063-2101, https://doi.org/10.1016/S1352-2310(99)00460-4, 2000.

Bates, K. H. and Jacob, D. J.: An Expanded Definition of the Odd Oxygen Family for Tropospheric Ozone Budgets: Implications for Ozone Lifetime and Stratospheric Influence, Geophys. Res. Lett., 47, e2019GL084486, https://doi.org/10.1029/2019gl084486, 2020.

Butler, T., Lupascu, A., and Nalam, A.: Attribution of ground-level ozone to anthropogenic and natural sources of nitrogen oxides and reactive carbon in a global chemical transport model, Atmos. Chem. Phys., 20, 10707-10731, https://doi.org/10.5194/acp-20-10707-2020, 2020.

Butler, T., Lupascu, A., Coates, J., and Zhu, S.: TOAST 1.0: Tropospheric Ozone Attribution of Sources with Tagging for CESM 1.2.2, Geosci. Model Dev, 11, 2825–2840, https://doi.org/10.5194/gmd-11-2825-2018, 2018.

Castellanos, P. and Boersma, K. F.: Reductions in nitrogen oxides over Europe driven by environmental policy and economic recession, Sci. Rep., 2, 265, https://doi.org/10.1038/srep00265, 2012.

Cheng, J., Tong, D., Liu, Y., Yu, S., Yan, L., Zheng, B., Geng, G., He, K., and Zhang, Q.: Comparison of current and future $PM_{2.5}$ air quality in China under CMIP6 and DPEC emission scenarios, Geophys. Res. Lett., 48, e2021GL093197, https://doi.org/10.1029/2021GL093197, 2021.

Collet, S., Kidokoro, T., Karamchandani, P., Jung, J., and Shah, T.: Future year ozone source attribution modeling study using CMAQ-ISAM, J. Air Waste Manag. Assoc., 68, 1239-1247, https://doi.org/10.1080/10962247.2018.1496954, 2018.

Cooper, O. R., Gao, R.-S., Tarasick, D., Leblanc, T., and Sweeney, C.: Long-term ozone trends at rural ozone monitoring sites across the United States, 1990-2010, J. Geophys. Res. Atmos., 117, D22307, https://doi.org/10.1029/2012JD018261, 2012.

Cooper, O. R., Schultz, M. G., Schröder, S., Chang, K.-L., Gaudel, A., Gerardo, Benítez, C., Cuevas, E., Fröhlich, M., Galbally, I. E., Kubistin, D., Lu, X., Audra, McClure-Begley, A., Molloy, S., Nédélec, P., O'Brien, J., Oltmans, S. J., Irina, Petropavlovskikh, I., Ries, L., Senik, I., Sjöberg, K., Solberg, S., Spain, T. G.,

Spangl, W., Steinbacher, M., Tarasick, D., Thouret, V., and Xu, X.: Multi-decadal surface ozone trends at globally distributed remote locations, Elem. Sci. Anth., 8, 23, https://doi.org/10.1525/elementa.420, 2020.

Clappier, A., Belis, C. A., Pernigotti, D., and Thunis, P.: Source apportionment and sensitivity analysis: two methodologies with two different purposes, Geosci. Model Dev., 10, 4245–4256, https://doi.org/10.5194/gmd-10-4245-2017, 2017.

Duncan, B. N., Lamsal, L. N., Thompson, A. M., Yoshida, Y., Lu, Z., Streets, D. G., Hurwitz, M. M., and Pickering, K. E.: A space-based, high-resolution view of notable changes in urban NO_x pollution around the world (2005–2014), J J. Geophys. Res. Atmos., 21, 976-996, https://doi.org/10.1002/2015JD024121, 2016.

Dunker, A. M., Yarwood, G., Ortmann, J. P., and Wilson, G. M.: Comparison of Source Apportionment and Source Sensitivity of Ozone in a Three-Dimensional Air Quality Model, Environ. Sci. Technol., 36, 2953–2964, https://doi.org/10.1021/es011418f, 2002.

Emmons, L. K., Hess, P. G., Lamarque, J.-F., and Pfister, G. G.: Tagged ozone mechanism for MOZART-4, CAM-chem and other chemical transport models, Geosci. Model Dev., 5, 1531–1542, https://doi.org/10.5194/gmd-5-1531-2012, 2012.

Emmons, L. K., Walters, S., Hess, P. G., Lamarque, J.-F., Pfister, G. G., Fillmore, D., Granier, C., Guenther, A., Kinnison, D., Laepple, T., Orlando, J., Tie, X., Tyndall, G., Wiedinmyer, C., Baughcum, S. L., and Kloster, S.: Description and evaluation of the Model for Ozone and Related chemical Tracers, version 4 (MOZART-4), Geosci. Model Dev., 3, 43–67, https://doi.org/10.5194/gmd-3-43-2010, 2010.

Eyring, V., Köhler, H. W., van Aardenne, J., and Lauer, A.: Emissions from international shipping: 1. The last 50 years, J. Geophys. Res., 110, D17305, https://doi.org/10.1029/2004JD005619, 2005.

Fan, T., Liu, X., Ma, P.-L., Zhang, Q., Li, Z., Jiang, Y., Zhang, F., Zhao, C., Yang, X., Wu, F., and Wang, Y.: Emission or atmospheric processes? An attempt to attribute the source of large bias of aerosols in eastern China simulated by global climate models, Atmos. Chem. Phys., 18, 1395–1417, https://doi.org/10.5194/acp-18-1395-2018, 2018.

Fiore, A. M., West, J. J., Horowitz, L. W., Naik, V., and Schwarzkopf, M. D.:

608 Characterizing the tropospheric ozone response to methane emission controls
609 and the benefits to climate and air quality, J. Geophys. Res., 113, D08307,
610 https://doi.org/10.1029/2007JD009162, 2008.
611
612 Fiore, A. M., Dentener, F. J., Wild, O., Cuvelier, C., Schultz, M. G., Hess, P.,
613 Textor, C., Schulz, M., Doherty, R. M., Horowitz, L. W., MacKenzie, I. A.,
614 Sanderson, M. G., Shindell, D. T., Stevenson, D. S., Szopa, S., van Dingenen,
615 R., Zeng, G., Atherton, C., Bergmann, D., Bey, I., Carmichael, G., Collins, W. J.,
616 Duncan, B. N., Faluvegi, G., Folberth, G., Gauss, M., Gong, S., Hauglustaine,
617 D., Holloway, T., Isaksen, I. S. A., Jacob, D. J., Jonson, J. E., Kaminski, J. W.,
618 Keating, T. J., Lupu, A., Marmer, E., Montanaro, V., Park, R. J., Pitari, G., Pringle,
619 K. J., Pyle, J. A., Schroeder, S., Vivanco, M. G., Wind, P., Wojcik, G., Wu, S.,
620 and Zuber, A.: Multimodel estimates of intercontinental source-receptor
621 relationships for ozone pollution, J. Geophys. Res., 114, D04301 ,
622 https://doi.org/10.1029/2008JD010816, 2009.
623
624 Fleming, Z. L., Doherty, R. M., Schneidemesser, E. V., Malley, C. S., Cooper, O.
625 R., Pinto, J. P., Colette, A., Xu, X., Simpson, D., Schultz, M. G., Lefohn, A. S.,
626 Hamad, S., Moolla, R., Solberg, S., and Feng, Z.: Tropospheric Ozone
627 Assessment Report: Present-day ozone distribution and trends relevant to
628 human health, Elem. Sci. Anth., 6, 12, https://doi.org/10.1525/elementa.273,
629 2018.
630
631 Gao, J., Zhu, B., Xiao, H., Kang, H., Hou, X., and Shao, P.: A case study of
632 surface ozone source apportionment during a high concentration episode,
633 under frequent shifting wind conditions over the Yangtze River Delta, China, Sci.
634 Total Environ., 544, 853-863, https://doi.org/10.1016/j.scitotenv.2015.12.039,
635 2016.
636
637 Gao, Y., Fu, J. S., Drake, J. B., Lamarque, J. F., and Liu, Y.: The impact of
638 emission and climate change on ozone in the United States under
639 representative concentration pathways (RCPs), Atmos. Chem. Phys., 13, 9607-
640 9621, https://doi.org/10.5194/acp-13-9607-2013, 2013.
641
642 Gaudel, A., Cooper, O. R. , Chang, K. L., Bourgeois, I., Ziemke, J. R., Strode,
643 S. A., Oman, L. D., Sellitto, P., Nédélec, P., Bolt, R., Thouret, V. and Granier,C.:
644 Aircraft observations since the 1990s reveal increases of tropospheric ozone at
645 multiple locations across the Northern Hemisphere, Sci. Adv., 6, eaba8272,
646 https://doi.org/10.1126/sciadv.aba8272, 2020.
647
648 Gelaro, R., McCarty, W., Suárez, M. J., Todling, R., Molod, A., Takacs, L.,
649 Randles, C. A., Darmenov, A., Bosilovich, M. G., Re- ichle, R., Wargan, K., Coy,

L., Cullather, R., Draper, C., Akella, S., Buchard, V., Conaty, A., da Silva, A. M., Gu, W., Kim, G., Koster, R., Lucchesi, R., Merkova, D., Nielsen, J. E., Partyka, G., Pawson, S., Putman, W., Rienecker, M., Schubert, S. D., Sienkiewicz, M., and Zhao, B.: The Modern-Era Retrospective Analysis for Research and Applications, Version 2 (MERRA-2), J. Climate, 30, 5419–5454, https://doi.org/10.1175/JCLI-D-16- 0758.1, 2017.

Grewe, V., Tsati, E., Mertens, M., Frömming, C., and Jöckel, P.: Contribution of emissions to concentrations: the TAGGING 1.0 submodel based on the Modular Earth Submodel System (MESSy 2.52), Geosci. Model Dev., 10, 2615–2633, https://doi.org/10.5194/gmd-10-2615-2017, 2017.

Haagen-Smit, A. J.: Chemistry and Physiology of Los Angeles Smog, Ind. Eng. Chem., 44, 1342-1346, https://doi.org/10.1021/ie50510a045, 1952.

Hodnebrog, Ø., Berntsen, T. K., Dessens, O., Gauss, M., Grewe, V., Isaksen, I. S. A., Koffi, B., Myhre, G., Olivié, D., Prather, M. J., Pyle, J. A., Stordal, F., Szopa, S., Tang, Q., van Velthoven, P., Williams, J. E., and Ødemark, K.: Future impact of non-land based traffic emissions on atmospheric ozone and OH – an optimistic scenario and a possible mitigation strategy, Atmos. Chem. Phys., 11, 11293–11317, https://doi.org/10.5194/acp-11-11293-2011, 2011.

Hoesly, R. M., Smith, S. J., Feng, L., Klimont, Z., Janssens-Maenhout, G., Pitkanen, T., Seibert, J. J., Vu, L., Andres, R. J., Bolt, R. M., Bond, T. C., Dawidowski, L., Kholod, N., Kurokawa, J.-I., Li, M., Liu, L., Lu, Z., Moura, M. C. P., O'Rourke, P. R., and Zhang, Q.: Historical (1750–2014) anthropogenic emissions of reactive gases and aerosols from the Community Emissions Data System (CEDS), Geosci. Model Dev., 11, 369–408, https://doi.org/10.5194/gmd-11-369-2018, 2018.

Han, H., Liu, J., Yuan, H., Zhuang, B., Zhu, Y., Wu, Y., Yan, Y., and Ding, A.: Characteristics of intercontinental transport of tropospheric ozone from Africa to Asia, Atmos. Chem. Phys., 18, 4251–4276, https://doi.org/10.5194/acp-18-4251-2018, 2018.

Hoor, P., Borken-Kleefeld, J., Caro, D., Dessens, O., Endresen, Ø., Gauss, M., Grewe, V., Hauglustaine, D. A., Isaksen, I. S. A., Jöckel, P., Lelieveld, J., Myhre, G., Meijer, E. W., Olivié, D., Prather, M. J., Poberaj, C. S., Shine, K. P., Staehelin, J., Tang, Q., Aardenne, J. v., Velthoven, P. F. J. v., and Sausen, R.: The impact of traffic emissions on atmospheric ozone and OH: results from QUANTIFY, Atmos. Chem. Phys., 9, 3113-3116, https://doi.org/10.5194/acp-9-3113-2009, 2009.

Jaffe, D. A., Cooper, O. R., Fiore, A. M., Henderson, B. H., Tonnesen, G. S., Russell, A. G., Henze, D. K., Langford, A. O., Lin, M., and Moore, T.: Scientific assessment of background ozone over the U.S.: Implications for air quality management, Elem. Sci. Anth, 6, 56, https://doi.org/ https://doi.org/10.1525/elementa.309, 2018.

Johnson, C., Collins, W., Stevenson, D., and Derwent, R.: Relative roles of climate and emissions changes on future tropospheric oxidant concentrations, J. Geophys. Res., 104, 18631–18645, https://doi.org/10.1029/1999JD900204, 1999.

Kasibhatla, P., Levy, H., Moxim, W. J., Pandis, S. N., Corbett, J. J., Peterson, M. C., Honrath, R. E., Frost, G. J., Knapp, K., Parrish, D. D., and Ryerson, T. B.: Do emissions from ships have a significant impact on concentrations of nitrogen oxides in the marine boundary layer?, Geophys. Res. Lett., 27, 2229–2232, https://doi.org/10.1029/2000gl011387, 2000.

Koo, B., Wilson, G. M., Morris, R., Dunker, A. M., and Yarwood, G.: Comparison of Source Apportionment and Sensitivity Analysis in a Particulate Matter Air Quality Model, Environ. Sci. Technol., 43, 6669–6675, https://doi.org/10.1021/es9008129, 2009.

Kwok, R. H. F., Baker, K. R., Napelenok, S. L., and Tonnesen, G. S.: Photochemical grid model implementation and application of VOC, NO_x, and O_3 source apportionment, Geosci. Model Dev., 8, 99–114, https://doi.org/10.5194/gmd-8-99-2015, 2015.

Lamarque, J.-F., Emmons, L. K., Hess, P. G., Kinnison, D. E., Tilmes, S., Vitt, F., Heald, C. L., Holland, E. A., Lauritzen, P. H., Neu, J., Orlando, J. J., Rasch, P. J., and Tyndall, G. K.: CAM-chem: description and evaluation of interactive atmospheric chemistry in the Community Earth System Model, Geosci. Model Dev., 5, 369–411, https://doi.org/10.5194/gmd-5-369-2012, 2012.

Lin, M., Fiore, A. M., Horowitz, L. W., Langford, A. O., Oltmans, S. J., Tarasick, D., and Rieder, H. E.: Climate variability modulates western U.S. ozone air quality in spring via deep stratospheric intrusions, Nat. Commun., 6, 7105, https://doi.org/10.1038/ncomms8105, 2015.

Lin, M., Horowitz, L. W., Payton, R., Fiore, A. M., and Tonnesen, G. S.: US surface ozone trends and extremes from 1980 to 2014: quantifying the roles of rising Asian emissions, domestic controls, wildfires, and climate, Atmos. Chem.

Phys., 17, 2943–2970, https://doi.org/10.5194/acp-17-2943-2017, 2017.

Lupaşcu, A. and Butler, T.: Source attribution of European surface O_3 using a tagged O_3 mechanism, Atmos. Chem. Phys., 19, 14535–14558, https://doi.org/10.5194/acp-19-14535-2019, 2019.

Mertens, M., Kerkweg, A., Grewe, V., Jöckel, P., and Sausen, R.: Attributing ozone and its precursors to land transport emissions in Europe and Germany, Atmos. Chem. Phys., 20, 7843–7873, https://doi.org/10.5194/acp-20-7843-2020, 2020.

McDuffie, E. E., Smith, S. J., O'Rourke, P., Tibrewal, K., Venkataraman, C., Marais, E. A., Zheng, B., Crippa, M., Brauer, M., and Martin, R. V.: A global anthropogenic emission inventory of atmospheric pollutants from sector- and fuel-specific sources (1970–2017): an application of the Community Emissions Data System (CEDS), Earth Syst. Sci. Data, 12, 3413–3442, https://doi.org/10.5194/essd-12-3413-2020, 2020.

Müller-Casseres, E., Edelenbosch, O. Y., Szklo, A., Schaeffer, R., and van Vuuren, D. P.: Global futures of trade impacting the challenge to decarbonize the international shipping sector, Energy, 237, 121547, https://doi.org/10.1016/j.energy.2021.121547, 2021

Myhre, G., D. Shindell, F.-M. Bréon, W. Collins, J. Fuglestvedt, J. Huang, D. Koch, J.-F. Lamarque, D. Lee, B. Mendoza, T. Nakajima, A. Robock, G. Stephens, T. Takemura and H. Zhang, 2013: Anthropogenic and Natural Radiative Forcing. In: Climate Change 2013: The Physical Science Basis. Contribution of Working Group I to the Fifth Assessment Report of the Intergovernmental Panel on Climate Change [Stocker, T.F., D. Qin, G.-K. Plattner, M. Tignor, S.K. Allen, J. Boschung, A. Nauels, Y. Xia, V. Bex and P.M. Midgley (eds.)]. Cambridge University Press, Cambridge, United Kingdom and New York, NY, USA, 2013.

Neu, J. L. and Prather, M. J.: Toward a more physical representation of precipitation scavenging in global chemistry models: cloud overlap and ice physics and their impact on tropospheric ozone, Atmos. Chem. Phys. Discuss., 11, 24413–24466, https://doi.org/10.5194/acpd-11-24413-2011, 2011

O'Neill, B. C., Tebaldi, C., van Vuuren, D. P., Eyring, V., Friedlingstein, P., Hurtt, G., Knutti, R., Kriegler, E., Lamarque, J.-F., Lowe, J., Meehl, G. A., Moss, R., Riahi, K., and Sanderson, B. M.: The Scenario Model Intercomparison Project (ScenarioMIP) for CMIP6, Geosci. Model Dev., 9, 3461-3482,

https://doi.org/10.5194/gmd-9-3461-2016, 2016.

Price, C., Penner, J., and Prather, M.: NO_x from lightning 1, Global distribution based on lightning physics, J. Geophys. Res., 102, 5929–5941, https://doi.org/10.1029/96JD03504, 1997.

Seinfeld, J. H. and Pandis, S. N.: Atmospheric Chemistry and Physics: From Air Pollution to Climate Change, J. Wiley, Hoboken, N.J., 2006.

Simon, H., Reff, A., Wells, B., Xing, J., and Frank, N.: Ozone trends across the United States over a period of decreasing NO_x and VOC emissions, Environ. Sci. Technol., 49, 186-195, https://doi.org/10.1021/es504514z, 2015.

Shen, L. and Mickley, L. J.: Effects of El Niño on summertime ozone air quality in the eastern United States, Geophys. Res. Lett., 44, 12543–12550, https://doi.org/10.1002/2017GL076150, 2017.

Stevenson, D. S., Dentener, F. J., Schultz, M. G., Ellingsen, K., van Noije, T. P. C., Wild, O., Zeng, G., Amann, M., Atherton, C. S., Bell, N., Bergmann, D. J., Bey, I., Butler, T., Cofala, J., Collins, W. J., Derwent, R. G., Doherty, R. M., Drevet, J., Eskes, H. J., Fiore, A. M., Gauss, M., Hauglustaine, D. A., Horowitz, L. W., Isaksen, I. S. A., Krol, M. C., Lamarque, J.-F., Lawrence, M. G., Montanaro, V., Müller, J.-F., Pitari, G., Prather, M. J., Pyle, J. A., Rast, S., Rodriguez, J. M., Sanderson, M. G., Savage, N. H., Shindell, D. T., Strahan, S. E., Sudo, K., and Szopa, S.: Multimodel ensemble simulations of present-day and near-future tropospheric ozone, J. Geophys. Res., 111, D08301. https://doi.org/10.1029/2005JD006338, 2006.

Sudo, K., and Akimoto, H.: Global source attribution of tropospheric ozone: Long-range transport from various source regions, J. Geophys. Res., 112, D12302, https://doi.org/10.1029/2006JD007992, 2007.

Szopa, S., Naik, V., Adhikary, B., Artaxo, P., Berntsen, T., Collins, W.D., Fuzzi, S., Gallardo, L., Kiendler-Scharr, A., Klimont, Z., Liao, H., Unger, N. and Zanis, P., 2021: Short-Lived Climate Forcers. In Climate Change 2021: The Physical Science Basis. Contribution of Working Group I to the Sixth Assessment Report of the Intergovernmental Panel on Climate Change [Masson-Delmotte, V., Zhai, P., Pirani, A., Connors, S.L., Péan, C., Berger, S., Caud, N., Chen, Y., Goldfarb, L., Gomis, M.I., Huang, M., Leitzell, K., Lonnoy, E., Matthews, J.B.R., Maycock, T.K., Waterfield, T., Yelekçi, O., Yu, R. and Zhou B. (eds.)]. Cambridge University Press, Cambridge, United Kingdom and New York, NY, USA, pp. 817–922, doi:10.1017/9781009157896.008, 2021.

Thor, R. N., Mertens, M., Matthes, S., Righi, M., Hendricks, J., Brinkop, S., Graf, P., Grewe, V., Jöckel, P., and Smith, S.: An inconsistency in aviation emissions between CMIP5 and CMIP6 and the implications for short-lived species and their radiative forcing, Geosci. Model Dev., 16, 1459–1466, https://doi.org/10.5194/gmd-16-1459-2023, 2023.

Thunis, P., Clappier, A., Tarrason, L., Cuvelier, C., Monteiro, A., Pisoni, E., Wesseling, J., Belis, C., Pirovano, G., Janssen, S., Guerreiro, C., and Peduzzi, E.: Source apportionment to support air quality planning: Strengths and weaknesses of existing approaches, Environ. Int., 130, 104825, https://doi.org/10.1016/j.envint.2019.05.019, 2019.

Tilmes, S., Lamarque, J. F., Emmons, L. K., Kinnison, D. E.,Marsh, D., Garcia, R. R., Smith, A. K., Neely, R. R., Conley, A., Vitt, F., V al Martin, M., Tanimoto, H., Simpson, I., Blake, D. R., and Blake, N.: Representation of the Community Earth System Model (CESM1) CAM4-chem within the Chemistry-Climate Model Initiative (CCMI), Geosci. Model Dev., 9, 1853–1890, https://doi.org/10.5194/gmd-9-1853-2016, 2016.

Tilmes, S., Lamarque, J. F., Emmons, L. K., Kinnison, D. E., Ma, P. L., Liu, X., Ghan, S., Bardeen, C., Arnold, S., Deeter, M., Vitt, F., Ryerson, T., Elkins, J. W., Moore, F., Spackman, J. R., and Val Martin, M.: Description and evaluation of tropospheric chemistry and aerosols in the Community Earth System Model (CESM1.2), Geosci. Model Dev., 8, 1395-1426, https://doi.org/10.5194/gmd-8-1395-2015, 2015.

van Marle, M. J. E., Kloster, S., Magi, B. I., Marlon, J. R., Daniau, A.-L., Field, R. D., Arneth, A., Forrest, M., Hantson, S., Kehrwald, N. M., Knorr, W., Lasslop, G., Li, F., Mangeon, S., Yue, C., Kaiser, J. W., and van der Werf, G. R.: Historic global biomass burning emissions for CMIP6 (BB4CMIP) based on merging satellite observations with proxies and fire models (1750–2015), Geosci. Model Dev., 10, 3329-3357, https://doi.org/10.5194/gmd-10-3329-2017, 2017.

von Glasow, R., Lawrence, M. G., Sander, R., and Crutzen, P. J.: Modeling the chemical effects of ship exhaust in the cloud-free marine boundary layer, Atmos. Chem. Phys., 3, 233–250, https://doi.org/10.5194/acp-3-233-2003, 2003.

Wang, H., Rasch, P. J., Easter, R. C., Singh, B., Zhang, R., Ma, P.-L., Qian, Y., Ghan, S. J., and Beagley, N.: Using an explicit emission tagging method in global modeling of source-receptor relationships for black carbon in the Arctic: Variations, sources, and transport pathways, J. Geophys. Res. Atmos., 119,

12888-12909, https://doi.org/10.1002/2014JD022297, 2014.

Wesely, M. L.: Parameterizations for surface resistance to gaseous dry deposition in regional-scale numerical models, Atmos. Environ., 23, 1293–1304, https://doi.org/10.1016/0004-6981(89)90153-4, 1989.

Xing, J., Pleim, J. E., Mathur, R., Pouliot, G., Hogrefe, C., Gan, C.-M., and Wei, C.: Historical gaseous and primary aerosol emissions in the United States from 1990 to 2010, Atmos. Chem. Phys., 13, 7531–7549, https://doi.org/10.5194/acp-13-7531-2013, 2013.

Yang, Y., Li, M., Wang, H., Li, H., Wang, P., Li, K., Gao, M., and Liao, H.: ENSO modulation of summertime tropospheric ozone over China, Environ. Res. Lett., 17, 034020, https://doi.org/10.1088/1748-9326/ac54cd, 2022.

Yang, Y., Liao, H., and Li, J.: Impacts of the East Asian summer monsoon on interannual variations of summertime surface-layer ozone concentrations over China, Atmos. Chem. Phys., 14, 6867–6879, https://doi.org/10.5194/acp-14-6867-2014, 2014.

Yang, Y., Wang, H., Smith, S. J., Zhang, R., Lou, S., Yu, H., Li, C., and Rasch, P. J.: Source apportionments of aerosols and their direct radiative forcing and long-term trends over continental United States, Earth's Future, 6, 793–808, https://doi.org/10.1029/2018EF000859, 2018.

Zhang, L., Jacob, D. J., Boersma, K. F., Jaffe, D. A., Olson, J. R., Bowman, K. W., Worden, J. R., Thompson, A. M., Avery, M. A., Cohen, R. C., Dibb, J. E., Flock, F. M., Fuelberg, H. E., Huey, L. G., McMillan, W. W., Singh, H. B., and Weinheimer, A. J.: Transpacific transport of ozone pollution and the effect of recent Asian emission increases on air quality in North America: an integrated analysis using satellite, aircraft, ozonesonde, and surface observations, Atmos. Chem. Phys., 8, 6117–6136, https://doi.org/10.5194/acp-8-6117-2008, 2008.

Zhang, Y., Cooper, O. R., Gaudel, A., Nedelec, P., Ogino, S. Y., Thompson, A. M., and West, J. J.: Tropospheric ozone change from 1980 to 2010 dominated by equatorward redistribution of emissions, Nat. Geosci., 9, 875-879, https://doi.org/10.1038/ngeo2827, 2016.

Zhang, Y., West, J. J., Emmons, L. K., Flemming, J., Jonson, J. E., Lund, M. T., Sekiya, T., Sudo, K., Gaudel, A., Chang, K. L., Nédélec, P., and Thouret, V.: Contributions of World Regions to the Global Tropospheric Ozone Burden Change From 1980 to 2010, Geophys. Res. Lett., 48, e2020GL089184,

902 https://doi.org/10.1029/2020GL089184, 2021.

Table 1. O_3 trends (ppb/decade) over eastern U.S. and western U.S. in winter (December-January-February, DJF) and summer (June-July-August, JJA) from observations and model simulations.

Season	Source	eastern U.S.	western U.S.
DJF	Observation	2.1 ± 0.29	2.2 ± 0.23
DJF	Model	6.1 ± 0.40	3.2 ± 0.28
JJA	Observation	-3.0±0.41	-0.5 ± 0.42
JJA	Model	-3.0±0.29	-2.3 ± 0.20

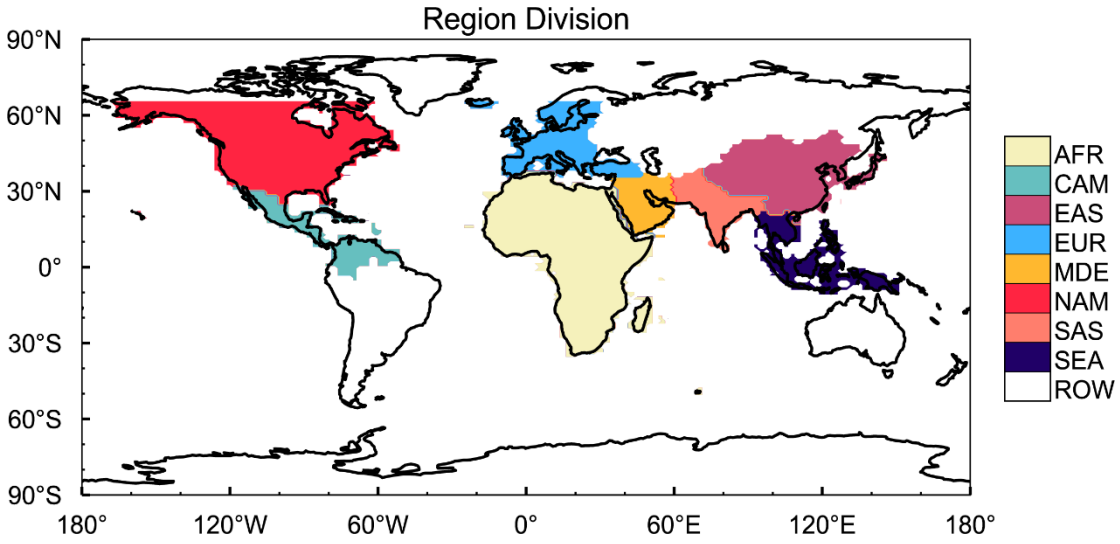

Figure 1. Source regions that are selected for O_3 source tagging in this study, include Africa (AFR), Central America (CAM), East Asia (EAS), Europe (EUR), Middle East (MDE), North America (NAM), South Asia (SAS), Southeast Asia (SEA) and rest of the world (ROW).

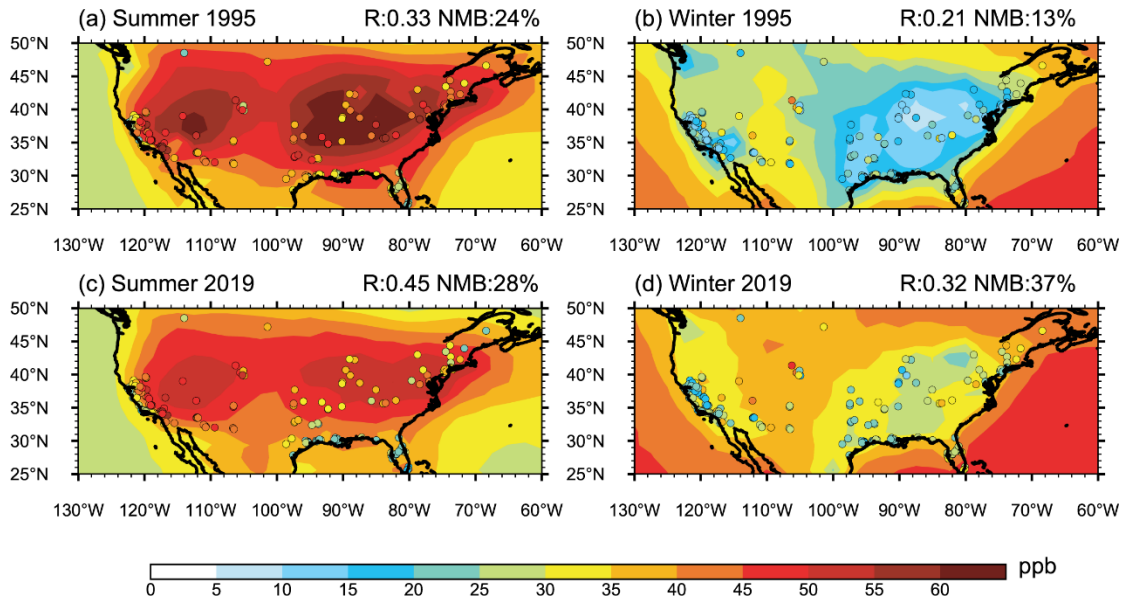

Figure 2. The simulated (contours) and observed (scatters) seasonal mean near-surface O3 mixing ratios over the United States in JJA (left) and DJF (right) and in 1995 (top) and 2019 (bottom). The correlation coefficient and normalized mean bias (NMB, $\sum$ (Model − Observation) / $\sum$ Observation × 100%) are shown on top right of each panel.

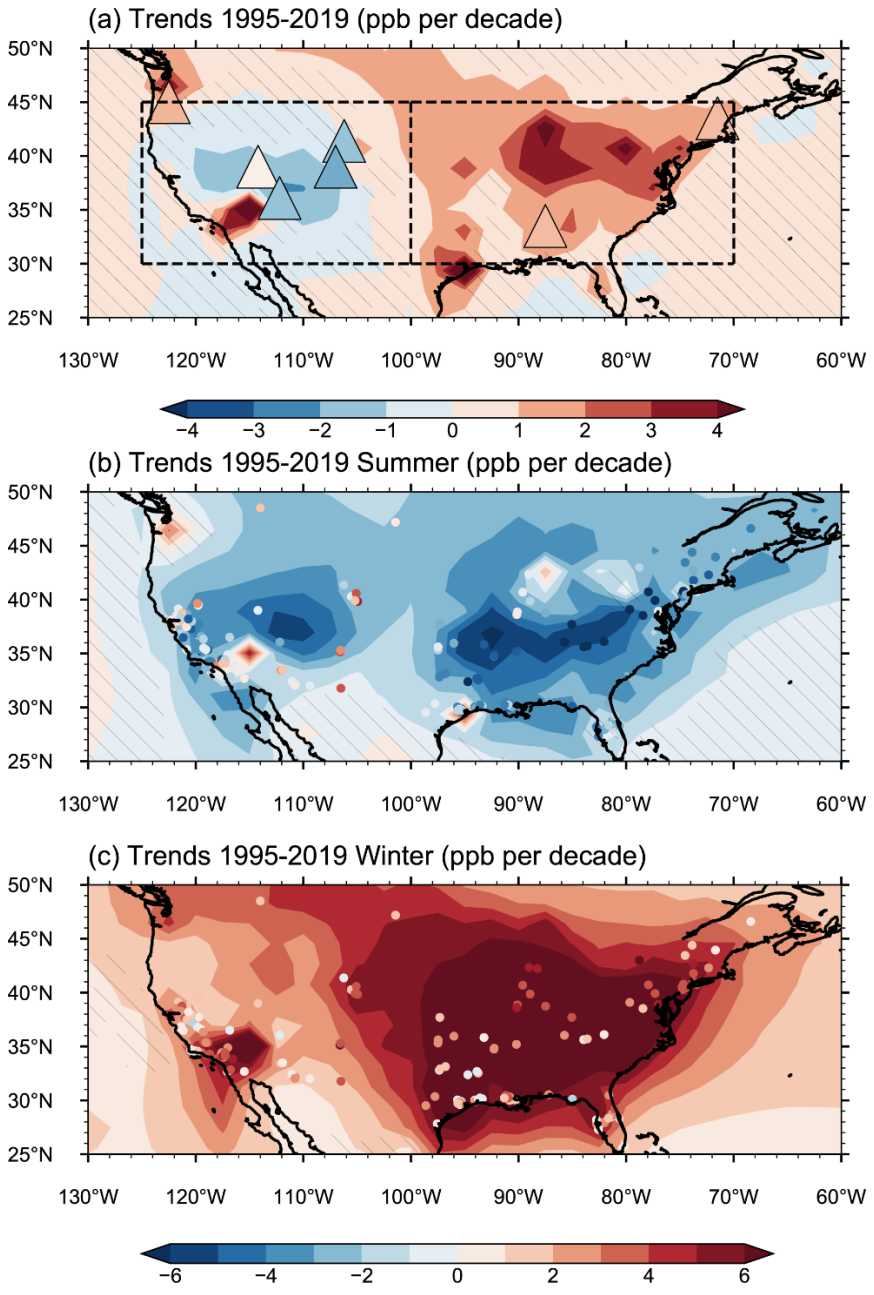

Figure 3. Linear trends (ppb/decade) of simulated (contours) and observed (color-filled markers) (a) annual, (b) JJA and (c) DJF mean near-surface O_3 mixing ratios during 1995–2019. Areas without hatches indicate statistical significance with 95% confidence. The boxes in (a) mark the western U.S. (WUS, 100–125°W, 30–45°N) and eastern U.S. (EUS, 70–100°W, 30–45°N), respectively. The observed annual O_3 mixing ratio trends in (a) are derived from IPCC AR6, based on Cooper et al. (2020) and Gaudel et al. (2020) over 1995–2017. The observed seasonal O_3 mixing ratio trends in (b) and (c) are calculated based on the U.S. EPA O_3 measurements over 1995–2019.

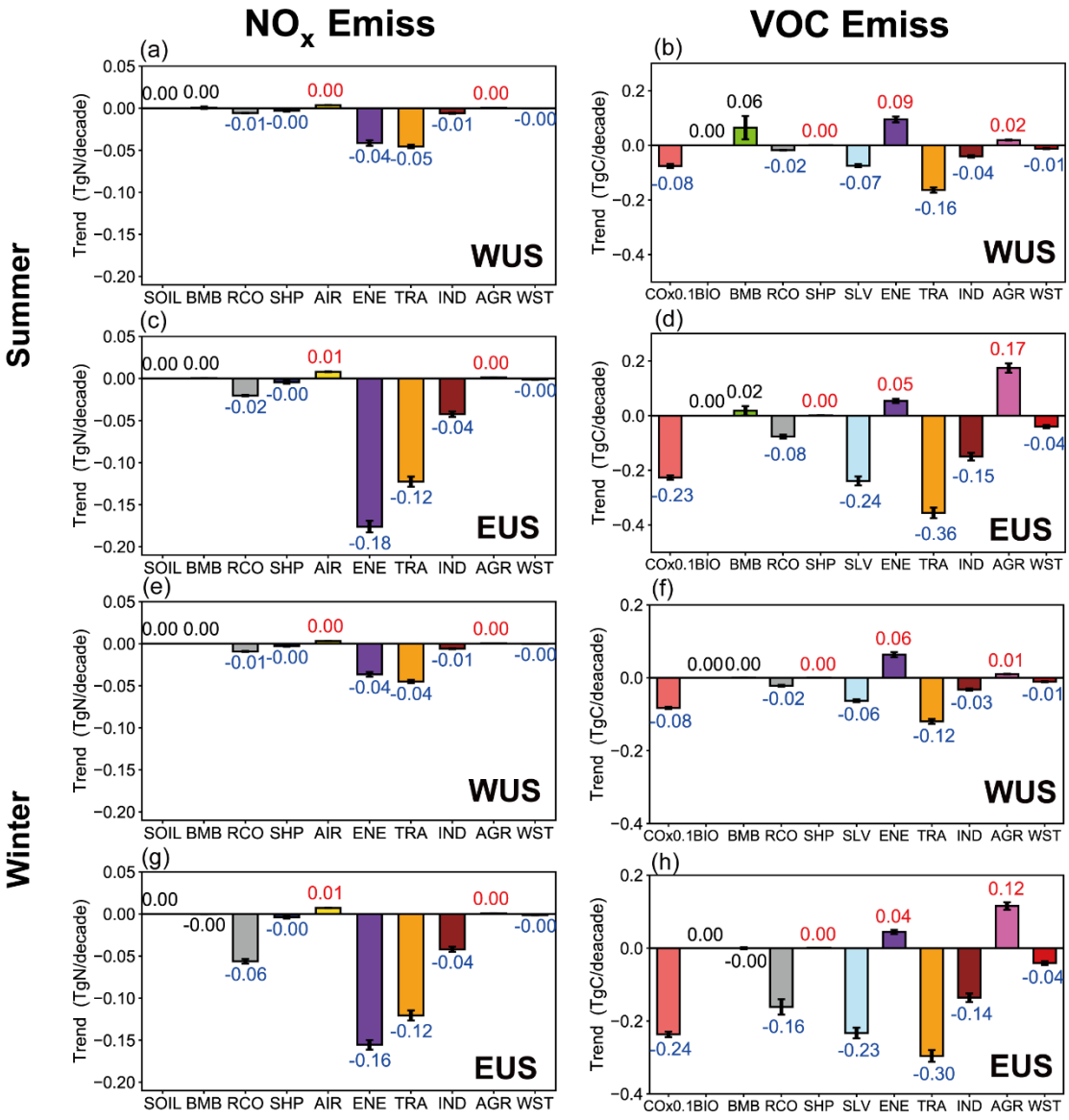

Figure 4. Linear trends of NO_x and reactive carbon emissions from various sectors in summer and winter over WUS and EUS. The increasing and decreasing trends marked with red and blue values, respectively, indicate statistical significance with 95% confidence.

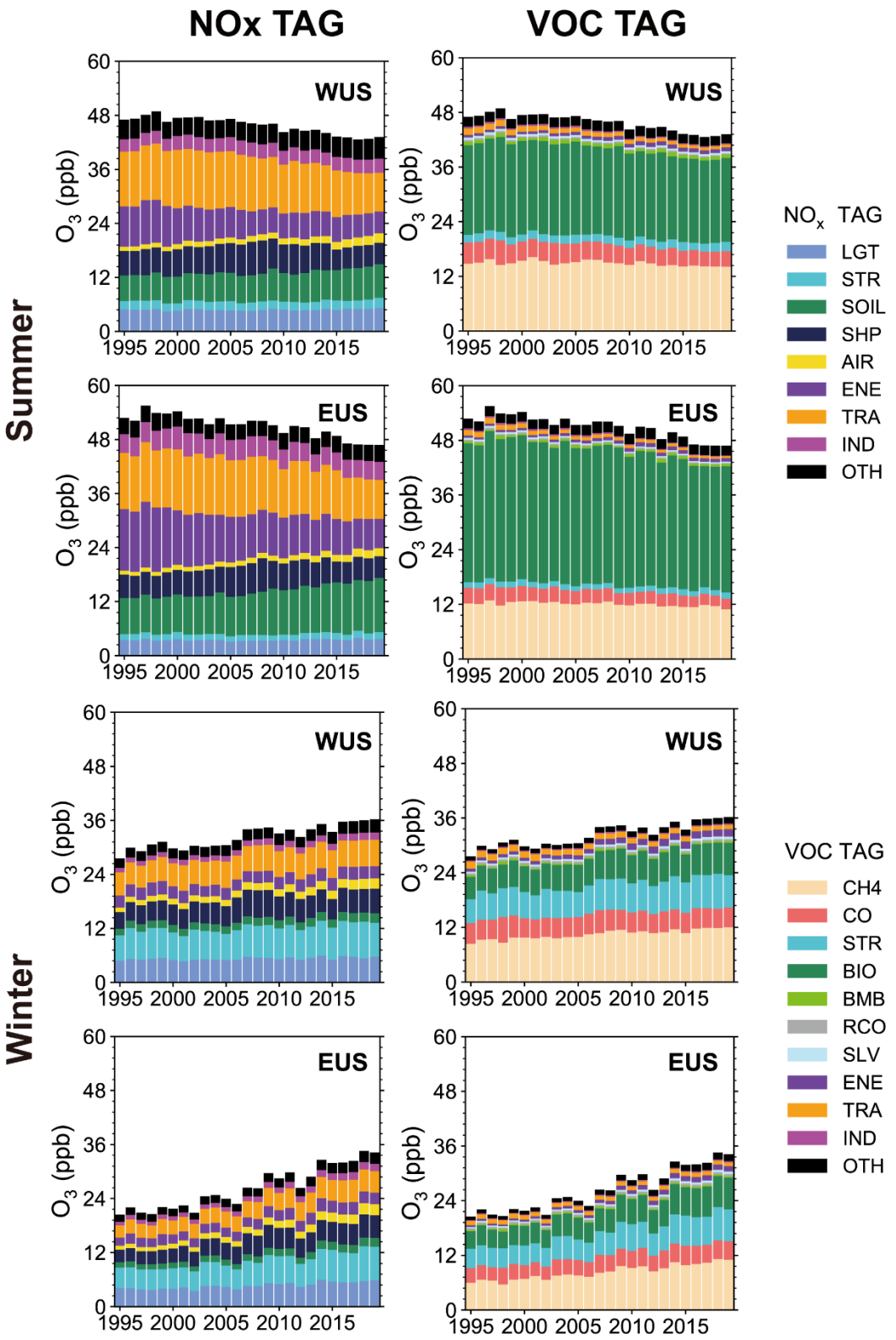

Figure 5. Time series of near-surface O_3 mixing ratios (ppb) averaged over WUS and EUS contributed by NO_x and reactive carbon emissions from different sectors in summer and winter during 1995–2019. Sources with small contributions are combined and shown as OTH.

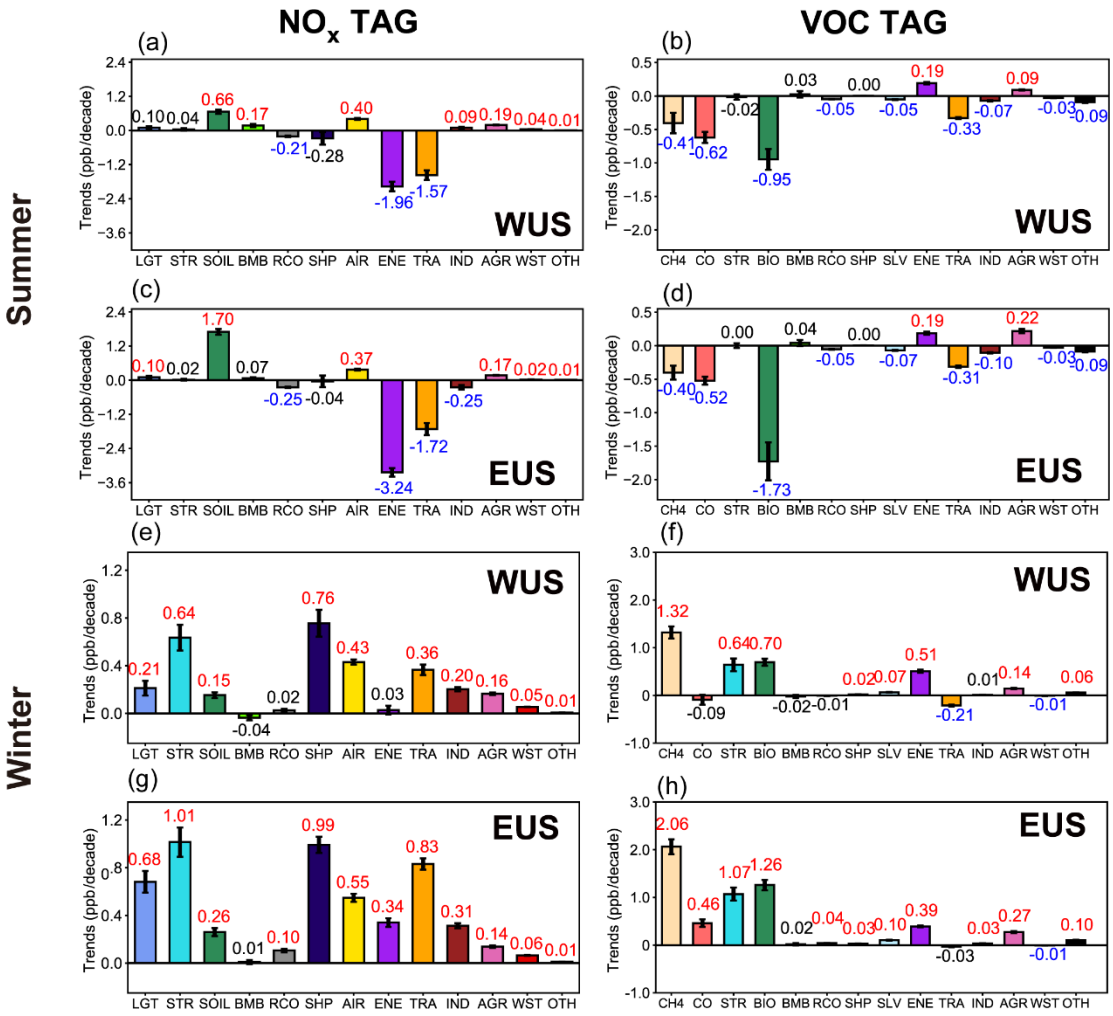

Figure 6. Linear trends (ppb/decade) of near-surface O_3 mixing ratios in summer and winter over WUS and EUS contributed by the NO_x (left) and reactive carbon (right) emissions from various sectors (color bars). The increasing and decreasing trends marked with red and blue color numbers, respectively, indicate statistical significance with 95% confidence. Other sources having small contributions are combined and shown as OTH.

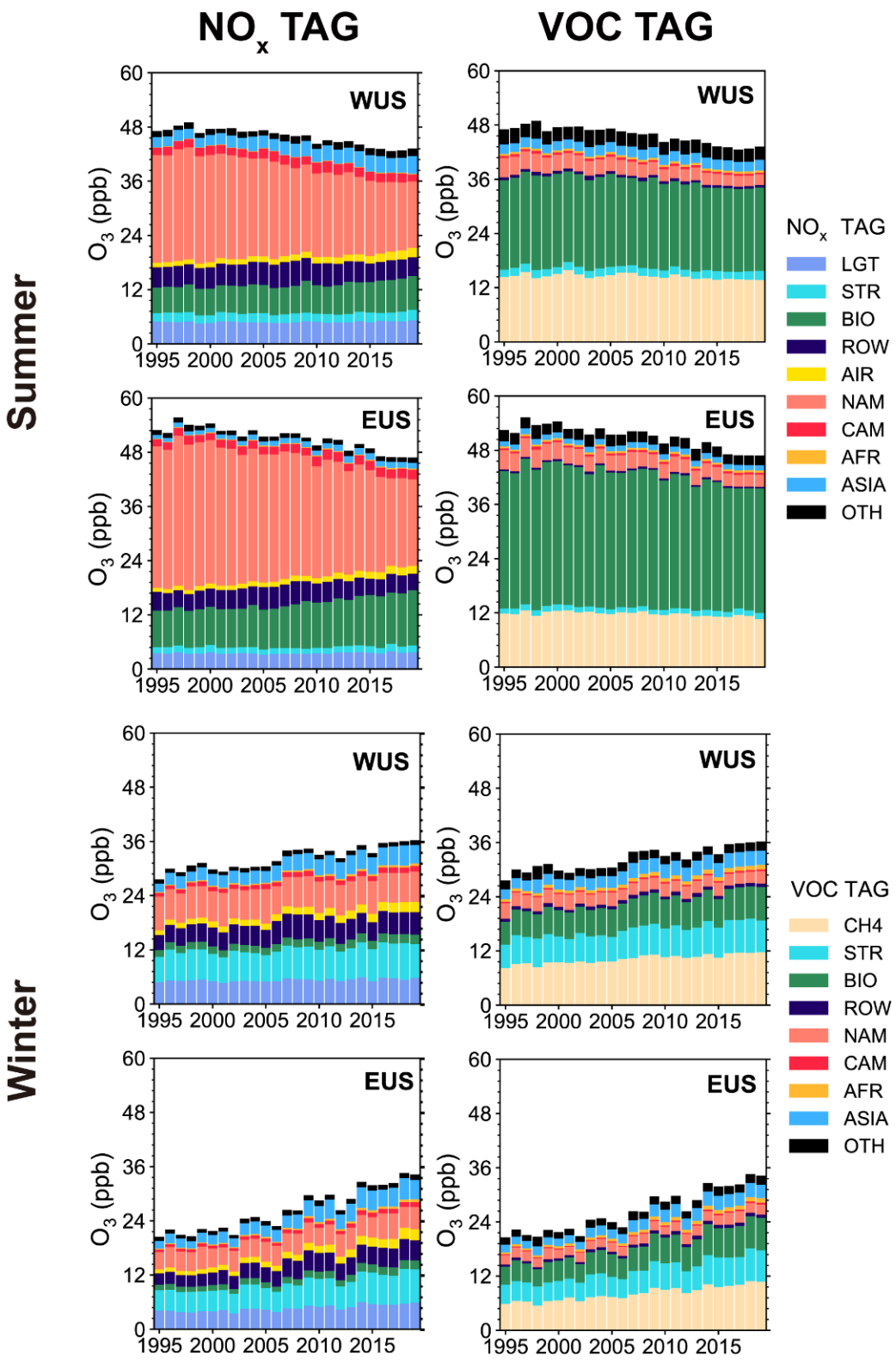

Figure 7. Time series of near-surface O_3 mixing ratios (ppb) averaged over WUS and EUS contributed by NO_x and reactive carbon emissions from different source regions in summer and winter during 1995–2019. Sources with small contributions are combined and shown as OTH.

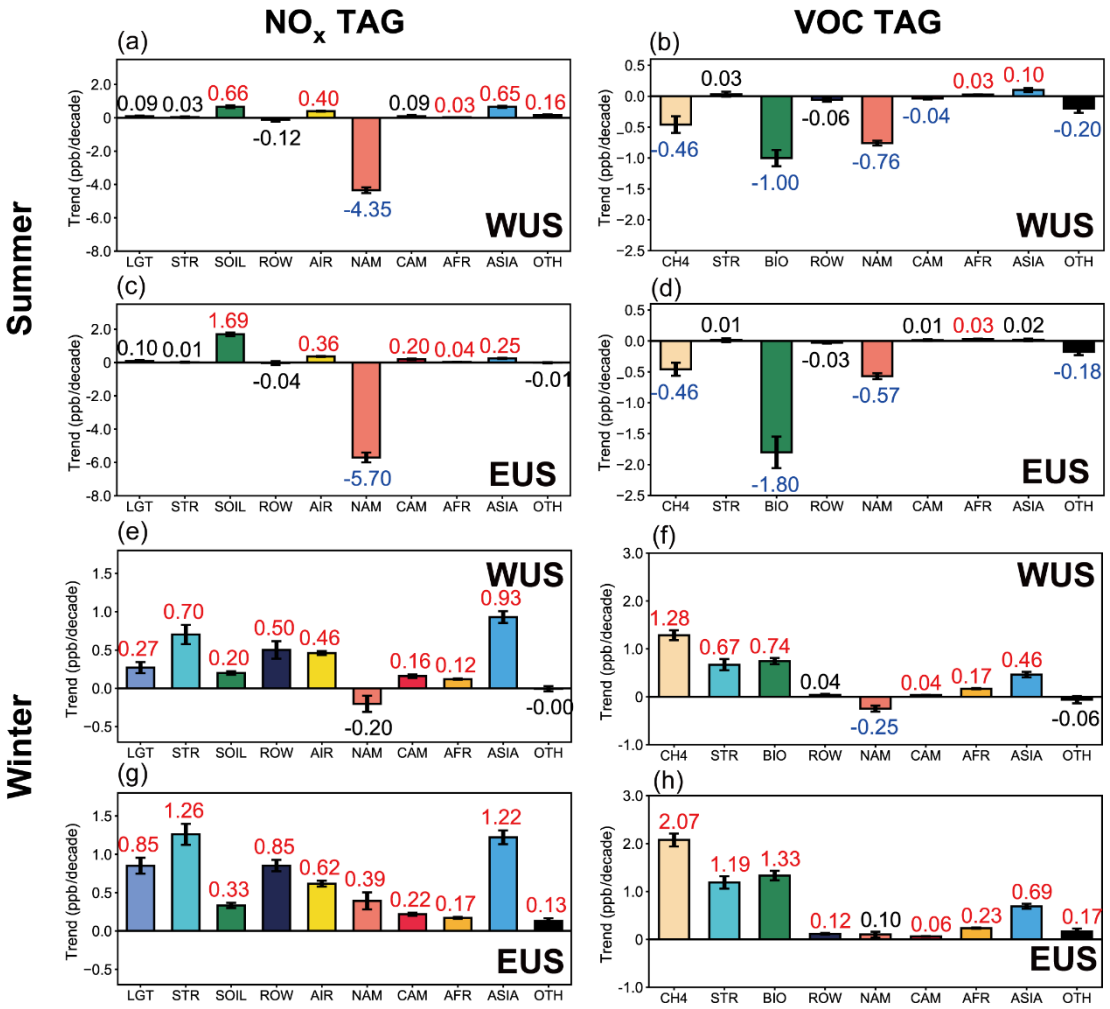

Figure 8. Linear trends (ppb/decade) of near-surface O_3 mixing ratios in summer and winter over WUS and EUS contributed by the NO_x (left) and reactive carbon (right) emissions from various source regions (color bars). The increasing and decreasing trends marked with red and blue color numbers, respectively, indicate statistical significance with 95% confidence. Contributions from source regions EAS, SAS and SEA are combined to ASIA. Other sources having small contributions are combined and shown as OTH.

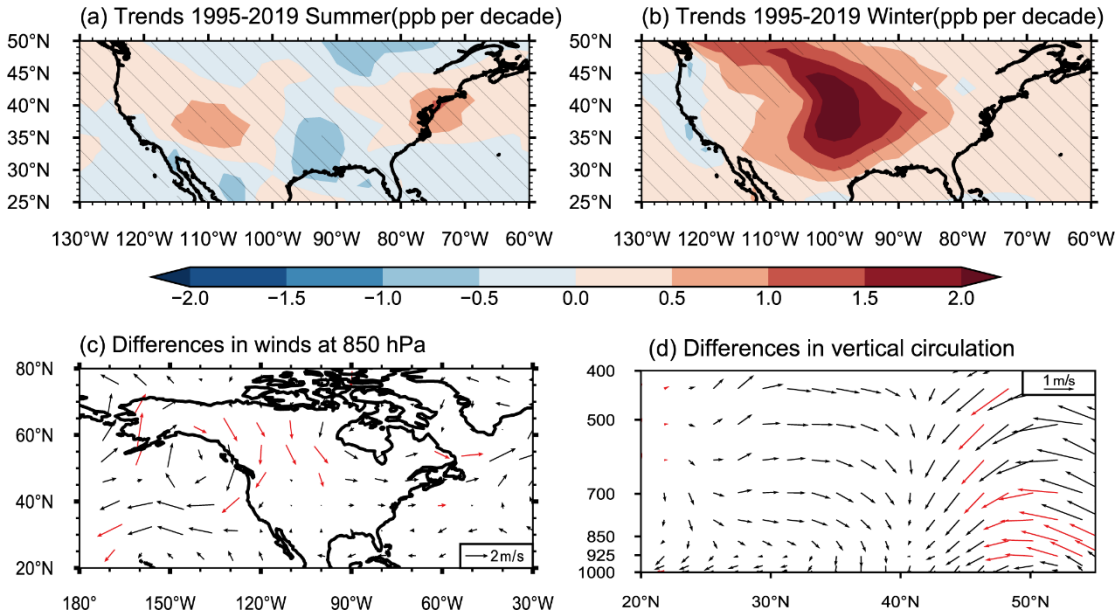

Figure 9. Linear trends (ppb/decade) of simulated (a) JJA and (b) DJF mean near-surface O_3 mixing ratios during 1995–2019. Differences between the first (1995–1999) and last (2015–2019) five years during 1995–2019 (last–first) in DJF mean (c) 850 hPa horizontal winds and (d) meridional winds and vertical velocity averaged over 90–105°W. Areas without hatches in (a) and (b) and red arrows in (c) and (d) indicate statistical significance with 95% confidence. All results are from the MET experiments.

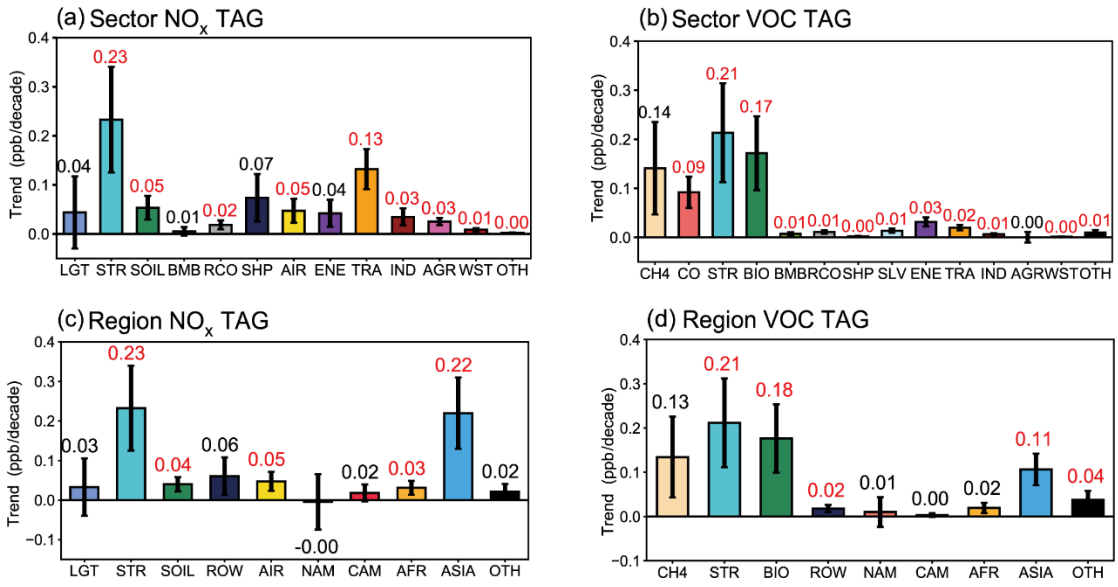

Figure 10. Linear trends (ppb/decade) of near-surface O_3 mixing ratios in winter over the U.S, contributed by the NO_x (a,c) and reactive carbon (b,d) emissions from various source sectors (a,b) and regions (c,d). The increasing and decreasing trends marked with red and blue color numbers, respectively, indicate statistical significance with 95% confidence. Contributions from source regions EAS, SAS and SEA are combined to ASIA. Some sources having small contributions are combined and shown as OTH.